Electronic Supplementary Material (ESI) for Inorganic Chemistry Frontiers.

Supporting Information for

Wheel-shaped molybdenum(V) cobalt-phosphate cluster as highly sensitive bifunctional photoelectrochemical sensor for the trace determination of Cr(VI) and tetracycline

Xiu-Juan Zhang, Yuan-Yuan Ma,* Hao-Xue Bi, Xiao-Yu Yin, Hao Song, Man-Hui Liu, Zhan-Gang Han*

Hebei Key Laboratory of Organic Functional Molecules; National Demonstration Center for Experimental Chemistry Education; College of Chemistry and Materials Science, Hebei Normal University, Shijiazhuang, Hebei 050024, Hebei 050024, P. R. China.

*Corresponding author email: mayy334@hebtu.edu.cn; hanzg116@126.com.

CONTENTS

1. Experimental section

1.1. Chemicals

All chemical reagents were obtained through commercial channels, and were used as received. Ultrapure water (18.25 MΩ cm) was obtained from a Sichuan-water-purifier physical and chemical analysis type water purifier (Sichuan, China) was used throughout the experiments unless otherwise noted. An aqueous solution of hexavalent chromium ions and tetracycline hydrochloride were prepared from potassium dichromate in ultrapure water. The lake water was first filtered to remove large particulate solid impurities and then acidified with H_2SO_4 to the pH equal to 0.3 (same as the pH of the 0.5 M H_2SO_4 electrolyte). $[(Mo_2O_4)_8(HPO_4)_{14}(PO_4)_{10}\{Co_{19}Na_4(H_2O)_{34}\}]\cdot 14\ H_2O$ (abbr. $Co_{16}Mo_{16}P_{24}$) was synthesized according to the previous reports.[1]

1.2. Synthesis of hybrid 1

A mixture of $Na_2MoO_4\cdot 2H_2O$ (0.10 g, 0.49 mmol), BBTZ (0.04 g, 0.17 mmol), $CoCl_2\cdot 6H_2O$ (0.20 g, 0.84 mmol), H_3PO_4 (0.50 mL, 7.50 mmol), and H_2O (8.00 mL, 0.44 mol) was stirred for 30 min, and the pH was adjusted to 2.0 with NaOH. The mixture was then transferred to a Teflon-lined reactor and kept at 160 ℃ for 5 days. After the reactor was cooled to room temperature at a rate of 10 ℃·h^{-1}, red bulk crystals of hybrid **1** was obtained, washed with distilled water and air dried to give a yield of 57% (based on Mo) (Fig. S1).

1.3. Instruments and measurements

The FT-IR spectrum (KBr precipitation) in the range of 4000~400 cm^{-1} was recorded with an FTIR-8900 infrared spectrometer. Powder X-ray diffraction (XRD) was performed on a Bruker AXSD8 Advance diffractometer. Scanning electron microscope images and Energy-dispersive spectroscopy (EDS) were conducted on a cold field emission scanning electron microscope (S-4800). Thermogravimetric (TG) analysis was carried out with a PerkinElmer Pyris Diamond TG Instruments. The UV-vis diffuse-reflectance spectroscopy (UV-vis DRS) spectra were characterized using an Agilent Cary 5000 UV-vis spectrophotometer with barium sulfate ($BaSO_4$) as the standard. All photoelectrochemical tests were completed using CHI760E workstation.

1.4. X-ray crystallography

Reliable diffraction data were collected using a Bruker APEX–II CCD diffractometer with Mo Kα monochromated radiation (λ =0.71073 Å) at 296(2) K. Using Olex2[2], the structure was solved with the SHELXT[3] structure solution

program using Intrinsic Phasing and refined with the SHELXL[4] refinement package using Least Squares minimisation. The CCDC codes are 2178098 for hybrid **1** Experimental sections

1.5. Electrochemical detection of Cr(VI) and tetracycline

All the electrochemical detection experiments were conducted on the CHI760E electrochemical workstation using a three-electrode system in 0.5 M H_2SO_4 (pH = 0). Cyclic voltammetry (CV) and electrochemical impedance spectroscopy (EIS) were used to characterize the electrochemical properties of hybrid **1**. EIS of the hybrid was tested at a frequency of 100 kHz to 1 Hz. The differential pulse voltammetry (DPV) technique was used to evaluate the electrochemical Cr(VI) and TC detection performance. For Cr(VI) detection, the potential window was set in the range of -0.1 ~ 0.8 V with amplitude of 50 mV. For TC detection, the potential window was in the range of -0.1 ~ 0.8 V with amplitude of 50 mV. The limit of detection of hybrid **1** was calculated according to the principle of S/N = 3. The relative standard deviation was calculated by using 15 cycles blank experiments. The detection sensitivity was obtained by linearly fitting the curves of Cr(VI)/TC concentration and corresponding peak currents. The actual water sample is first filtered out of impurities and then acidified as electrolyte for the photoelectrochemical detection experiments. The concentrations of added test substance (Cr(VI) and TC) range from 0.1 μM to 1.0 μM.

1.6. Preparation of working electrodes modified with hybrid 1

Before each experiment, the glass carbon electrode (GCE, diameter 3 mm) was polished on a polishing pad with 0.3 and 0.05 μm alumina powders. The cleaned GCE electrode was dried with nitrogen stream for the next modification. 12 mg of crystal was first mixed and grinded with carbon black under mass ratios of 1:2, and then dispersed into 200 μL of 0.5 wt% Nafion solution and ultrasonicated for 30 min to obtain a uniformly dispersed solution. Then, 12 μL of catalyst suspension was dropped on the surface of GCE electrodes and dried in air for testing. The Nafion solution acts as adhesive and the protecting agent to ensure that the hybrids catalysts can be tightly modified on the surface of GCE electrode.

2. Supplementary structural figures

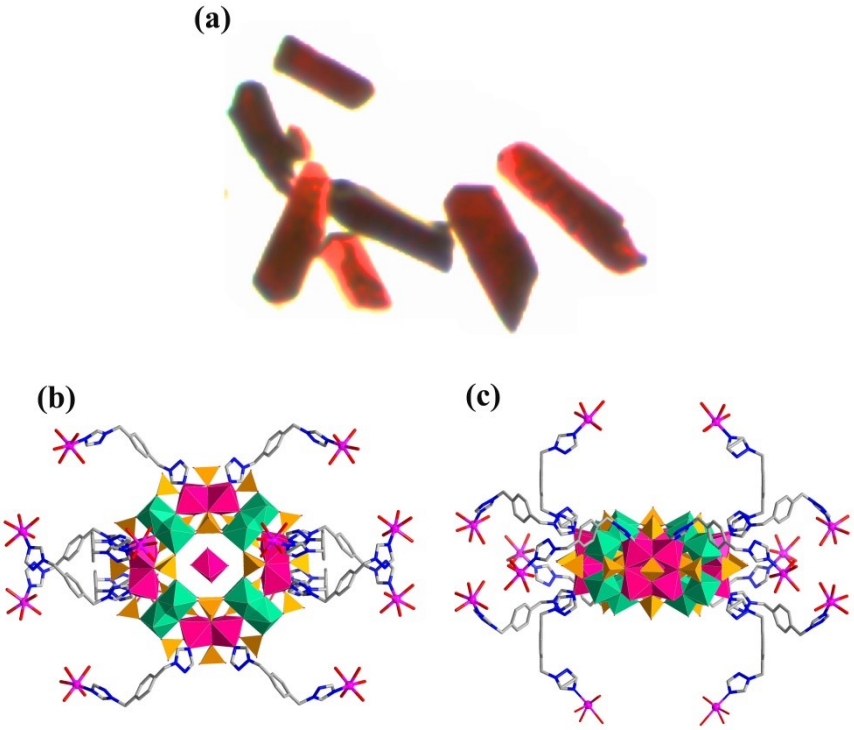

Figure S1 (a) The optical picture of hybrid **1;** (b-c) The twelve node positive representation of wheel-shaped $\{Co_{16}Mo_{16}P_{24}\}$ cluster in hybrid **1.**

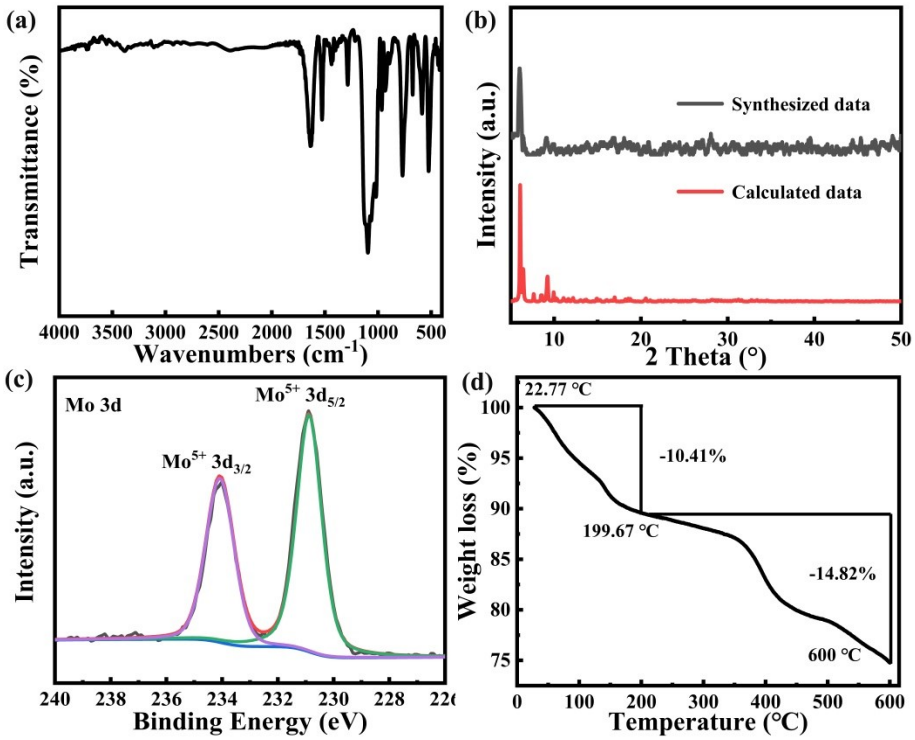

Figure S2 (a) IR spectrum of **1** showing the organic components; (b) The simulated and calculated XRD patterns of crystal **1**; (c) The high-resolution XPS spectrum of Mo in hybrid **1**; (d) The TG curves of hybrid **1** shows two weight loss steps corresponding to the loss of water molecules and organic species, and the weight loss is almost consistent with the weight loss calculated according to the crystal structure.

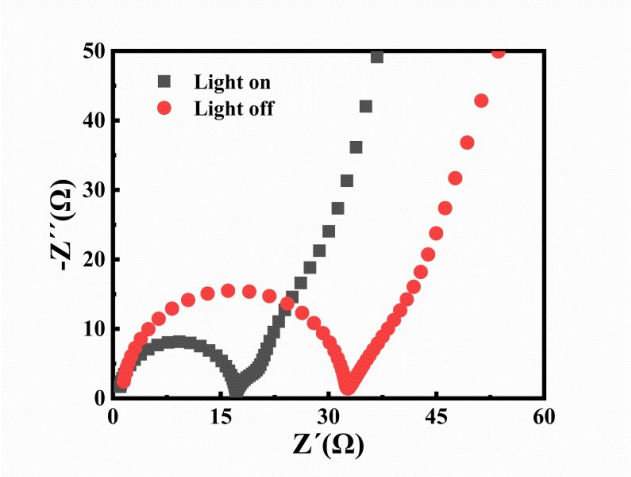

Figure S3 EIS spectra of hybrid **1** in dark and light-irradiation condition.

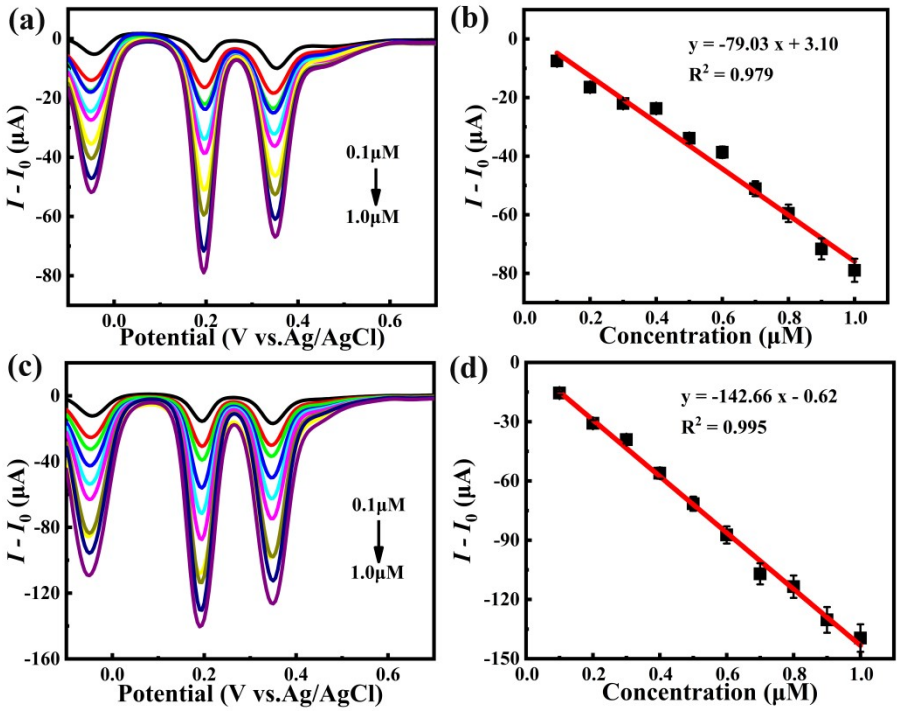

Figure S4 (a) DPV curves of $\{Co_{16}Mo_{16}P_{24}\}$ cluster modified electrodes in 0.5 M H_2SO_4 with continuous additions of Cr(VI) under dark condition; (b) The corresponding linear dependences; (c) DPV curves of $\{Co_{16}Mo_{16}P_{24}\}$ cluster in 0.5 M H_2SO_4 with the successive changes of 0.1 and 1.0 μM Cr(VI) under visible light illumination; (d) The linear dependence curve of $\{Co_{16}Mo_{16}P_{24}\}$ cluster.

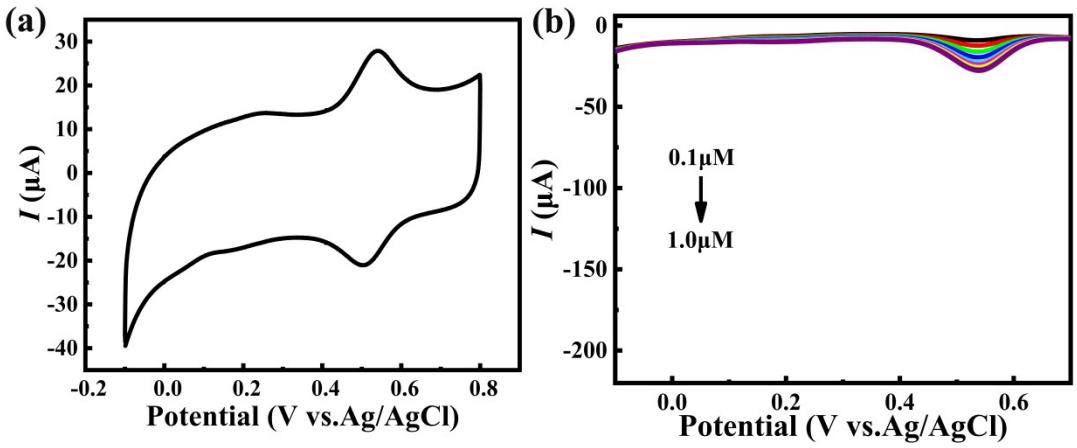

Figure S5 (a) CV curve of BBTZ ligand. (b) DPV curves of BBTZ ligand in 0.1-1.0 μM Cr(VI).

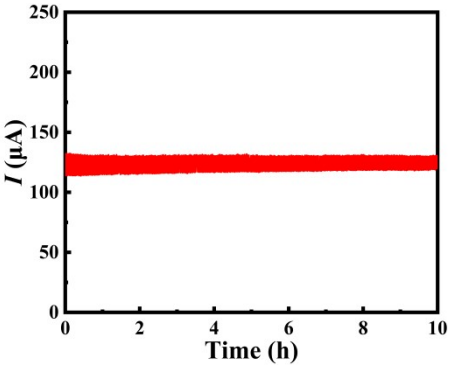

Figure S6 Amperometric responses for compound **1** to 50 μM Cr(VI) in 0.5 M H_2SO_4 electrolyte.

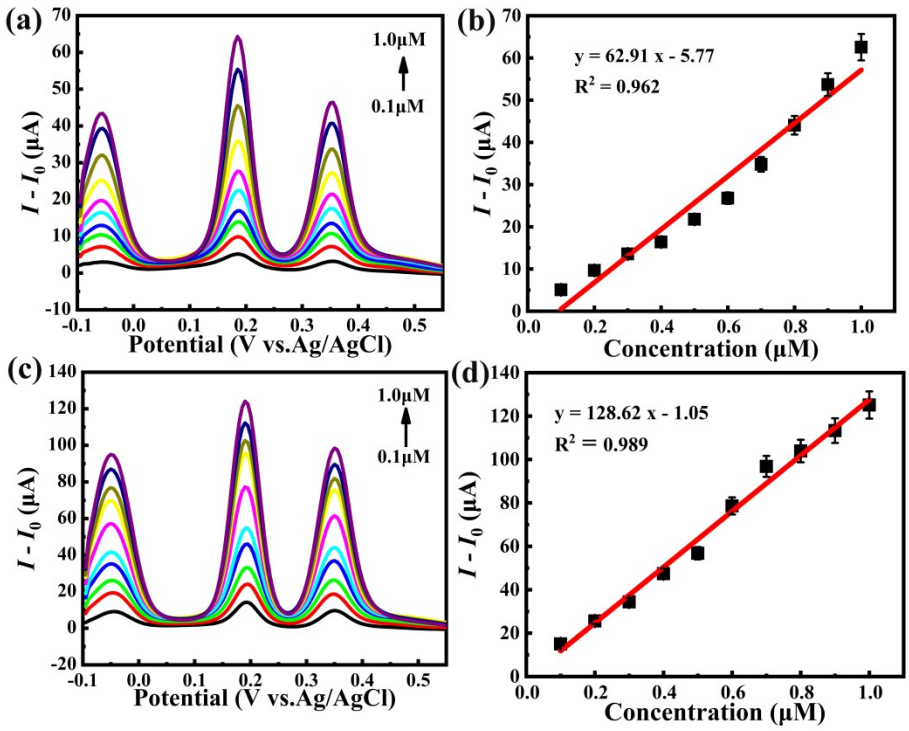

Figure S7 (a) DPV curves of $\{Co_{16}Mo_{16}P_{24}\}$ cluster modified electrodes in 0.5 M H_2SO_4 with continuous additions of TC under dark condition; (b) Corresponding linear dependence plot of $\{Co_{16}Mo_{16}P_{24}\}$ cluster; (c) DPV curves of $\{Co_{16}Mo_{16}P_{24}\}$ cluster in 0.5 M H_2SO_4 with the addition of 0.1 and 1.0 μM TC under visible light illumination; (d) Corresponding linear dependence plot under the visible light illumination.

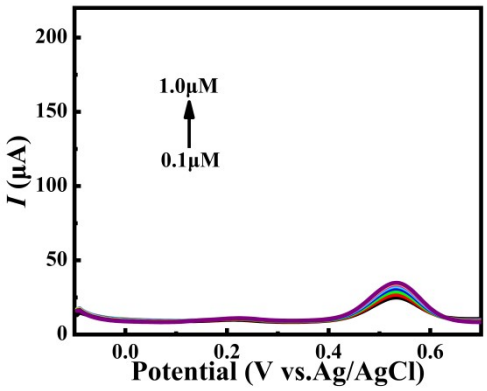

Figure S8 DPV curves of BBTZ ligand with 0.1-1.0 μM TC.

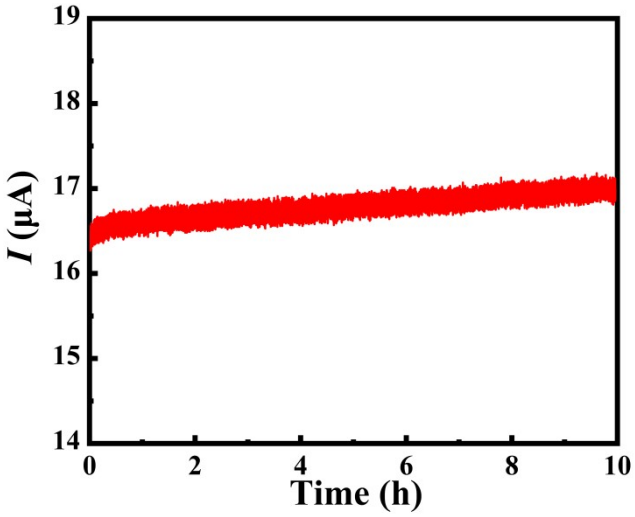

Figure S9 Amperometric responses for compound **1** to 50μM TC in 0.5 M H_2SO_4 electrolyte.

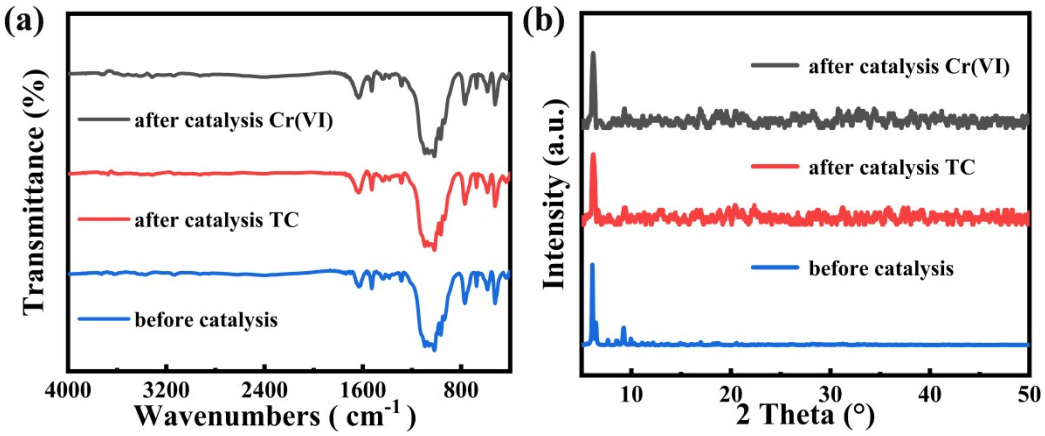

Figure S10 Comparisons of IR (a) and XRD (b) of compound **1** before and after catalysis reaction.

3. Supplementary structural tables

Table S1. Crystal data and structure refinement for Compound **1**

Hybrid	**1**
Empirical formula	$C_{72}H_{80}Co_{17}Mo_{16}N_{36}O_{142}P_{24}$
Formula weight	7001.85
Crystal system	triclinic
Space group	P-1
a (Å)	16.106(18)
b (Å)	19.486(20)
c (Å)	21.27(2)
α, β, γ (°)	107.40(2), 101.00(3), 113.34(3)
Volume (Å^3), *Z*	5474(10), 1
Density (calculated)	2.124
Reflections collected	27091
F(000)	3391.0
Crystal size (mm^3)	0.2×0.15×0.13
Goodness-of-fit on F^2	1.115
Final *R* indices [$I>2\sigma(I)$]	R_1 = 0.1163, wR_2 = 0.3016
R indices (all data)	R_1 = 0.1506, wR_2 = 0.3342

$R_1 = \sum (|F_o| - |F_c|) / \sum |F_o|$; $wR_2 = \{ \sum [w (|F_o|^2 - |F_c|^2)^2] / \sum [w (|F_o|^2)^2] \}^{1/2}$.

Table S2. The selected bond lengths (Å) of hybrid **1**

Mo1-Mo14	2.611(4)	Co9-N1	2.37(4)
Mo1-O8	1.918(14)	Co10-O10	2.040(14)
Mo1-O10	1.949(14)	Co10-O14[1]	2.115(14)
Mo1-O28	2.061(15)	Co10-O20[1]	2.091(14)
Mo1-O62[1]	2.087(14)	Co10-N1	2.106(19)
Mo2-Mo3	2.66(3)	Co11-P2	2.65(4)
Mo9-O54	2.24(2)	P1-O16	1.513(14)
Mo10-O24	2.015(14)	P1-O38	1.525(14)
Mo10-O27	2.385(14)	P1-O45	1.601(14)
Co2-O11	1.63(4)	N16-C35	1.44(3)
Co2-O15	1.98(4)	N17-C31	1.29(3)
Co3-O55	2.30(3)	C1-C23	1.42(3)
Co3-N4	2.41(3)	C2-C6	1.32(3)
O10-Mo1-O62[1]	88.4(6)	O6-Co12-O19	99.0(6)
O22-Mo1-Mo14	89.9(4)	O6-Co12-O23	170.9(6)
O21-Mo2-P4	104.8(10)	O20-Co13-O49	145.9(15)
O57-P4-Mo2	110.4(8)	N10[2]-Co14-O19	100.7(7)

[1]1-X, 1-Y, -Z.

Table S3. The selected bond angles (°) of compound **1**

Mo2-P4-O40-Co3	-9(3)	O42-P7-O58-Mo14	-70.4(13)
Mo3-Mo2-O56-P4	-6(4)	O42-P7-O58-Mo21	-69.7(13)
Mo7-P4-O56-Mo23	169.7(15)	O42-P7-O58-Mo22	-83(2)
Mo9-Mo19-O18-P12	-60(2)	O43-Mo3-O6-Mo2	-93.5(14)
Co9-N1-C8-N5	178.4(18)	O47-Mo24-O4-Mo18	-65.9(14)
Co9-N1-C31-N17	-174(2)	O47-Mo24-O12-P8	-80.6(18)
Co14[1]-N10-C27-N11	-158.9(17)	O50-Mo3-O6-Mo2	2.2(15)
Co15[4]-P10-O34-Co24	47.9(16)	O50-Mo11-O60-P12	48(3)
O2-P2-O72-Mo20	-167.5(15)	O56-P4-O40-Co12	-20.6(14)
O3-Mo21-O8-Mo7	89.9(14)	O56-P4-O40-Co18	149.5(10)
O41-Mo15-O48-Mo20	-84(2)	C31-N1-C8-N5	7(3)
O41-Mo15-O48-Co2	70(4)	C33-N4-C11-N9	-9(3)
O42-P7-O15-Co2	-31.0(18)	C34-C4-C20-C28	1(4)
O42-P7-O15-Co6	-12.7(13)	C35-N16-C24-N6	172(2)

[1]2-X, 2-Y, 1-Z; [4]1-X, 1-Y, -Z.

Table S4. BVS calculation results of atoms.

Hybrid	Mo1	Mo2	Mo3	Mo4	Mo5	Mo6	Mo7	Mo8
1	5.47	5.55	5.14	5.75	5.35	5.31	5.41	5.24

Table S5. Peak potential data (mV) for **1** at a sweep rate of 110 mV s^{-1}.

Scan rate	***E*a/*E*c (I) / mV**	***E*a/*E*c (II) / mV**	***E*a/*E*c (III) / mV**
110 mV s^{-1}	$E_{1/2}$	$E_{1/2}$	$E_{1/2}$
Hybrid 1	106/-273	255/-251	246/-214
	189.5	253	230

Concretely, the possible reaction for each reversible redox peaks are as follows:[5, 6]

$[(Mo_2O_4)_8(HPO_4)_{22}(PO_4)_2Co_4(H_2O)_8]^{26-} + 2e^- + 2H^+ = [H_2(Mo_2O_4)_8(HPO_4)_{22}(PO_4)_2Co_4(H_2O)_8]^{26-}$ (1)

$[H_2(Mo_2O_4)_8(HPO_4)_{22}(PO_4)_2Co_4(H_2O)_8]^{26-} + 2e^- + 2H^+ = [H_4(Mo_2O_4)_8(HPO_4)_{22}(PO_4)_2Co_4(H_2O)_8]^{26-}$ (2)

$[H_4(Mo_2O_4)_8(HPO_4)_{22}(PO_4)_2Co_4(H_2O)_8]^{26-} + 2e^- + 2H^+ = [H_6(Mo_2O_4)_8(HPO_4)_{22}(PO_4)_2Co_4(H_2O)_8]^{26-}$ (3)

References

1. C. du Peloux, A. Dolbecq, P. Mialane, J. Marrot, E. Rivière and F. Sécheresse, A New Family of Layered Molybdenum(V) Cobalto-Phosphates Built up of $[H_{14}(Mo_{16}O_{32})Co_{16}(PO_4)_{24}(H_2O)_{20}]_{10-}$ Wheels, *Angew. Chem. Int. Ed.*, 2001, **40**, 2455-2457.
2. O. V. Dolomanov, L. J. Bourhis, R. J. Gildea, J. A. K. Howard and H. Puschmann, Olex2: a complete structure solution, refinement and analysis program, *J Appl Crystallogr*, 2009, **42**, 339-341.
3. G. Sheldrick, Shelxt - Integrated space-group and crystal-structure determination, *Acta crystallographica. Section A*, 2015, **71**, 3-8.
4. G. Sheldrick, Crystal structure refinement with shelxt, *Acta Crystallogr. C*, 2015, **71**, 3-8.
5. U. Kei, I. Atuko, I. Eiki and T. Nobuyuki, Catalytic effects of chlorate ions on the electrode reaction processes of 12-molybdophosphate and 12-molybdosilicate, *Bull. Chem. Soc. Jpn*, 1984, **57**, 597-598.
6. L. Duan, F. Liu, X. Wang, E. Wang, C. Qin, Y. Li, X. Wang and C. Hu, A new 3D cadmium molybdenum phosphate with intersecting tunnels: hydrothermal synthesis, structure and electrochemical properties of $[C_3H_{12}N_2]_4[CdMo_{12}O_{24}(HPO_4)_6(PO_4)_2(OH)_6][(Cd(H_2O)_2]\cdot 3H_2O$, *J MOL STRUCT*, 2004, **705**, 15-20.